Spatial-fringe-modulation-based quality map for phase unwrapping

Quan, Chenggen; Tay, Cho Jui; Chen, Lujie; Fu, Yu

2003

Quan, C., Tay, C. J., Chen, L., & Fu, Y. (2003). Spatial-fringe-modulation-based quality map for phase unwrapping. Applied Optics, 42(35), 7060-7065.

https://hdl.handle.net/10356/91920

https://doi.org/10.1364/AO.42.007060

Spatial-fringe-modulation-based quality map for phase unwrapping

Chenggen Quan, Cho Jui Tay, Lujie Chen, and Yu Fu

The quality-guided algorithm is a method widely used in phase unwrapping. The algorithm uses a quality map to guide its unwrapping process, and its validity depends on whether the quality map can truly reflect phase quality. In fringe projection surface profilometry, discontinuous surface structure, low surface reflectivity, and saturation of the image-recording system are sources of unreliable phase data. To facilitate the unwrapping process, we demonstrate an accurate quality map based on spatial fringe modulation, which is extracted from a single fringe pattern. Compared with temporal fringe modulation, the new criterion is more sensitive to spatial structure changes and less dependent on illumination conditions. © 2003 Optical Society of America

OCIS codes: 120.5050, 120.2650, 120.2830.

1. Introduction

The phase-shifting technique,[1–3] well known for its high accuracy, is widely used in phase extraction. The phase obtained is wrapped by a factor of 2π and can be made continuous by a phase unwrapping process. However, many factors, such as discontinuous surface structure, low surface reflectivity, or saturation of image-recording system, would produce unreliable phase data, which make the recovery of a true phase profile challenging. The assignment of phase unwrapping algorithms is to remove 2π jumps from a wrapped phase map and confine unavoidable errors caused by unreliable phase data to minimum area.

Many unwrapping algorithms[4,5] have been developed in the past 20 years. Each proposes to solve some sorts of problem and each has its own drawbacks. Goldstein[6] proposed a block-path method based on the fact that most unreliable phase data function as residues in a phase map. The algorithm connects positive and negative residues by a so-called branch cut and unwraps the given phase map following a path without crossing any branch cut. Although branch cuts are effective in balancing residues, they may separate the phase map into several discrete parts, which would result in a discontinuous phase profile.

An alternative method is to minimize the influence of unreliable phase data indirectly. Instead of balancing residues, a quality map is applied to guide the unwrapping process. Bone[7] first incorporate phase quality into phase unwrapping by means of a quality mask. This was followed by the work of Quiroga *et al.*,[8] Lim *et al.*,[9] Yu and Cummings,[10] and Roth,[11] where the quality-guided algorithm was developed from a quality mask to an adaptive algorithm without the need of a threshold. The successful implementation of the method largely relies on the accuracy of the quality map. Depending on the application, several quality maps, such as those derived from correlation coefficients,[11] the variance of phase derivatives,[12] or fringe modulation,[13,14] were used by different authors.

Generally, in the phase-shifting technique, unreliable phase data are confined to those areas with low reflectivity, where the fringe modulation values are also low. Hence fringe modulation is naturally considered a good phase-quality indicator, with which the quality-guided unwrapping algorithm can retrieve a continuous phase profile. Ströbel[13] has also shown that fringe modulation can be used not only to determine an optimal unwrapping path but also to process phase data such as filtering, improving visualization, and masking. Despite its merits, fringe modulation has mainly two disadvantages. First, it is insensitive to shadowless surface structure change because low fringe modulation would be confined only

The authors are with the Department of Mechanical Engineering, National University of Singapore, 10 Kent Ridge Crescent, Singapore 119260. C. Quan's e-mail address is mpeqcg@nus.edu.sg.

Received 27 March 2003; revised manuscript received 6 August 2003.

0003-6935/03/357060-06$15.00/0

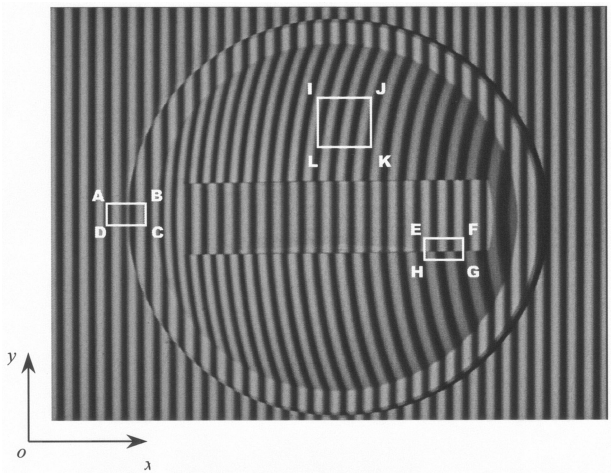

Fig. 1. Frame of projected fringe pattern.

to those areas with low reflectivity. If the illumination condition is such that some surface structure changes, such as step changes, do not cast a shadow, the values of fringe modulation would be high, even though phase data are unreliable. Secondly, fringe modulation must be derived from a number of phase-shifted images, making it inapplicable for dynamic measurement when only one phase image is recorded. In fact, the disadvantages arise from conventional or temporal fringe modulation (TFM), in which each point is extracted from several temporally distributed grey levels at the same position; therefore the spatial connections between a point under consideration and its neighboring points are not reflected. However, it is found that spatial connection is equally important to TFM in determining the reliability of phase data. This paper presents a spatial fringe modulation (SFM) technique derived from a single fringe pattern and shows that SFM is a good phase-quality indicator. Experimental results of the proposed method are compared with those obtained by block-path and TFM-guided phase unwrapping algorithms.

2. Principle of the Method

A. Spatial Fringe Modulation

The SFM of a point under consideration is calculated from $N \times M$ pixel grey levels. If the fringe pattern projected on an object surface is sinusoidal, as shown in Fig. 1, the light intensity in a $N \times M$ pixel window with point (x, y) at the center can be expressed as

$$I(i, j) = A(x, y) + B(x, y)\cos[i2\pi f + \theta(i, j)], \quad (1)$$

where i ranges from $x - N/2$ to $x + N/2$ and j from $y - M/2$ to $y + M/2$. $A(x, y)$ is the spatial illumination intensity, $B(x, y)$ is the SFM, $\theta(i, j)$ is a surface-height-related phase, and f is the projected fringe frequency along the x axis. For the fringe pattern shown in Fig. 1, the frequency f is 0.045

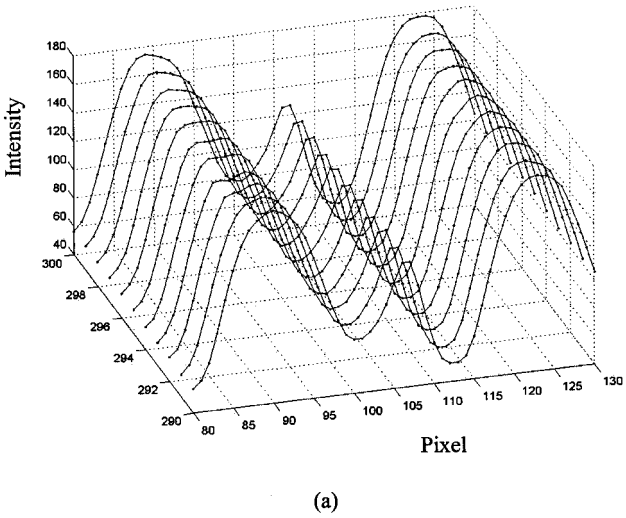

(a)

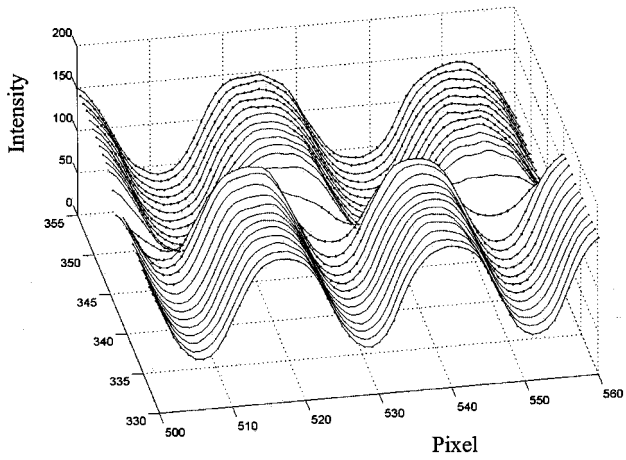

(b)

Fig. 2. 3D plot of pixels' grey level (a) in the area *ABCD* of Fig. 1, (b) in the area *EFGH* of Fig. 1.

cycle/pixel. The SFM is derived by the least-squares method. We can rewrite Eq. (1) as

$$I(i, j) = a_0(x, y) + a_1(x, y)\cos(i2\pi f) + a_2(x, y)\sin(i\delta), \quad (2)$$

where

$$\begin{aligned} a_0(x, y) &= A(x, y), \\ a_1(x, y) &= B(x, y)\cos\theta(i, j), \\ a_2(x, y) &= -B(x, y)\sin\theta(i, j). \end{aligned} \quad (3)$$

The square error $E(x, y)$ is given by

$$E(x, y) = \sum_{i=x-N/2}^{x+N/2} \sum_{j=y-M/2}^{y+M/2} [a_0(x, y) + a_1(x, y)\cos(i2\pi f) + a_2(x, y)\sin(i2\pi f) - g(i, j)]^2, \quad (4)$$

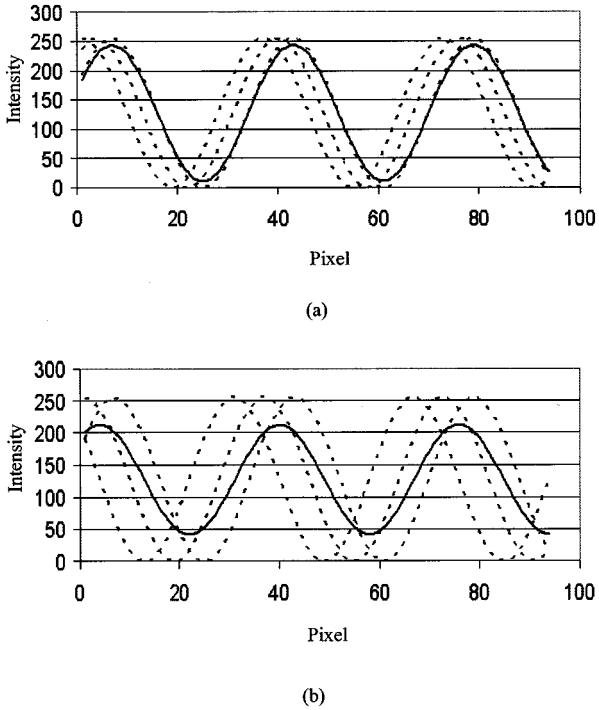

Fig. 3. (a) Effect of a 30° phase shift along the y axis on SFM; (b) Effect of a 60° phase shift along the y-axis on SFM.

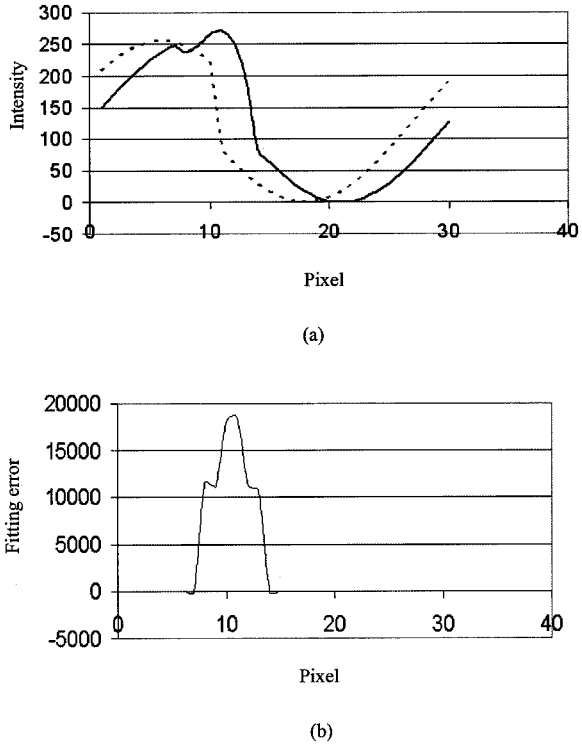

Fig. 4. (a) Effect of 60° phase shift along the x axis on SFM; (b) Fitting error of 60° phase shift along the x axis.

where $g(i,j)$ represents the grey level at point (i,j). A necessary condition for the minimum error $E(x, y)$ is

$$\frac{\partial E(x, y)}{\partial a_0(x, y)} = 0, \qquad \frac{\partial E(x, y)}{\partial a_1(x, y)} = 0, \qquad \frac{\partial E(x, y)}{\partial a_2(x, y)} = 0. \tag{5}$$

On the basis of Eq. (5), three unknowns, $a_0(x, y)$, $a_1(x, y)$, and $a_2(x, y)$ can be obtained. The SFM is given by

$$B(x, y) = [a_1^2(x, y) + a_2^2(x, y)]^{1/2}. \tag{6}$$

Generally, SFM is affected by two factors: the reflectivity of an object surface and the phase shift introduced in a fringe pattern. The first factor functions similarly in SFM and TFM, where high reflectivity results in large values of SFM and low reflectivity results in small values. The second is related to the spatial structure of an object surface. Wherever there is a sharp change in surface height, such as a step change, a phase shift would be introduced. Figures 2(a) and 2(b) are the three-dimensional (3D) plots of the two sections *ABCD* and *EFGH* in Fig. 1. Each shows a phase shift introduced by a step change along the x axis [Fig. 2(a)] or y axis [Fig. 2(b)].

The effect of a phase shift along the y axis on SFM is presented graphically in Fig. 3. Three dotted sinusoidal curves, shown in Fig. 3(a), represent the pixels' grey level on three adjacent horizontal lines, each having a 30° phase shift. The solid sinusoidal curve is obtained by least-squares error. The SFM, as shown by the amplitude of the solid curve, is slightly lower than the fringe modulation of the dotted curves. In Fig. 3(b) a 60° phase shift is introduced between the dotted curves. The corresponding least-squares-error fitted solid curve shows a significant decrease in the SFM value. This shows that SFM value decreases with the phase shift introduced along the y axis.

However, the relation between phase shift along the x axis and SFM is not as straightforward. Figure 4(a) shows a dotted sinusoidal curve with 60° phase shift introduced at $x = 10$, and the solid sinusoidal curve is the least-squares-error fitted result. It can be seen that the SFM shows a slight decrease followed by an increase around $x = 10$, and its value is approximately the same as the fringe modulation of the dotted curve. This indicates that SFM is not sensitive to a phase shift along the x axis; therefore an additional criterion must be developed to complement SFM. Li[14] proposed a fitting-error criterion to complement TFM to ensure phase reliability. It is found that the method is applicable to the problem under consideration. If $a_0(x, y)$, $a_1(x, y)$, and $a_2(x, y)$ obtained in Eq. (5), are substituted into Eq. (4) to obtain $E(x, y)$, a fitting error map that would identify the reliability of the corresponding phase map is obtained. Figure 4(b) shows the fitting error of the dotted curve in Fig. 4(a). The maximum error is found at $x = 10$, where the 60° phase shift is introduced. Integrating SFM with the fitting error, a modified reliability criterion $R(x, y)$ is defined as[14]

$$R(x, y) = \frac{B(x, y)}{1 + c\,[E(x, y)/B(x, y)]}, \tag{7}$$

where c is an adjustable variable related to $E(x, y)$.

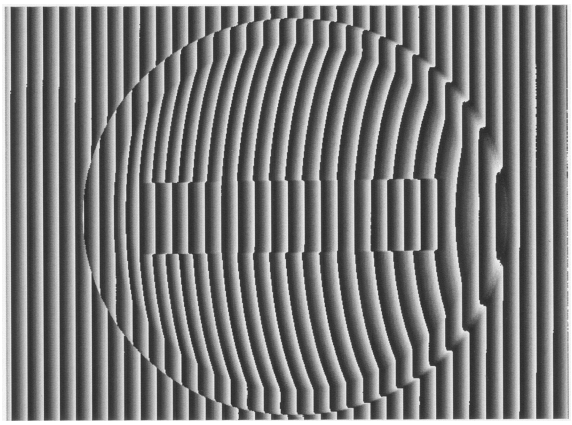

Fig. 5. Wrapped phase map of the hemisphere specimen.

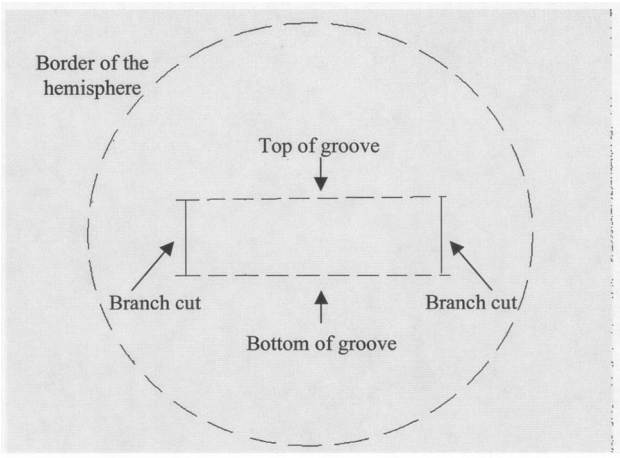

(a)

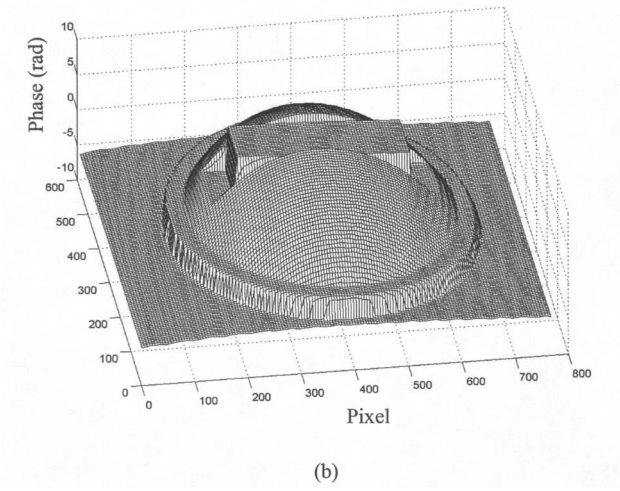

(b)

Fig. 6. (a) Branch cuts and (b) 3D plot shape generated by the block-path method.

B. Quality-Guided Phase Unwrapping

A quality map consists of arrays of values that define the quality of each pixel in a phase map. Different methods can be used to generate different quality maps. Some quality maps are derived from a wrapped phase map, whereas others, such as TFM or SFM maps, are extracted directly from the data from which a wrapped phase map is derived. Regardless of how a quality map is derived, the algorithms that uses the quality map to guide phase unwrapping are similar.

A detailed quality-guided phase unwrapping algorithm can be found in Ref. 5; the fringe-modulation-based phase unwrapping algorithm is a type of quality-guided phase unwrapping algorithm. The fringe modulation based algorithm unwraps the high-modulation phase at an early stage and the low-modulation phase at a later stage so that low-modulation data will not affect high-modulation data. The algorithm does not consider the influence of residues. Instead it is based on the assumption that an accurate fringe modulation map will provide a guide on an unwrapping path without encircling any unbalanced residues, which would introduce further errors.

3. Results and Discussion

A. Selection of Pixel Window Size

The SFM of a point under consideration is obtained from the grey levels of a $N \times M$ pixel window. The window size has a significant influence on the measurement accuracy of phase quality. For vertical fringe patterns, the pixel window height M should be small (3 or 5 is recommended). If M is large, the accumulated phase shift in the y direction would be very large, which would result in low SFM even for a high-quality phase point. Rectangle $IJKL$ in Fig. 1 can be used to exemplify the drawbacks of a large M. The specimen surface profile is continuous within $IJKL$ with high phase quality. However, the convex surface introduces a monotonically increasing phase shift in adjacent lines. If a large M were used, despite the trivial phase shift between adjacent lines, the accumulated phase shift would be very large, and the SFM would be mistakenly labeled as low quality. If a small M were used, the accumulated phase shift would be small and would not have a significant effect on SFM value, as shown in Fig. 3(a).

Similar to the parameter M, which dictates the number of sampling points used to evaluate phase shift in the y direction, the window width N dictates the number of points used to evaluate large phase shift in the x direction. As mentioned in the Section 2, SFM alone is not sensitive to phase shift in the x direction, while the square error $E(x, y)$ is. If N is arbitrarily set to three, no errors caused by the x-direction phase shift would be detectable, because three points are the minimum data necessary for solving for the three unknowns $a_0(x, y)$, $a_1(x, y)$, and $a_2(x, y)$ in Eq. (2); $E(x, y)$ obtained from Eq. (4) would reflect only the errors caused by phase shift in the y direction. Hence N should be relatively large to ensure sufficient sampling in the x direction; and $E(x, y)$

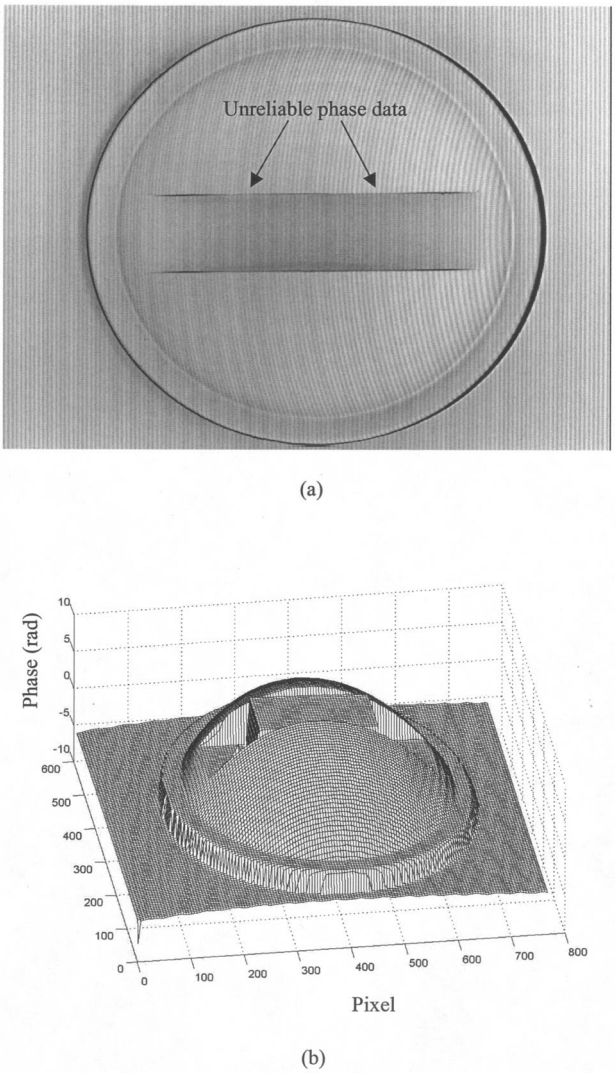

Fig. 7. (a) TFM map; (b) 3D plot shape generated by TFM-guided unwrapping.

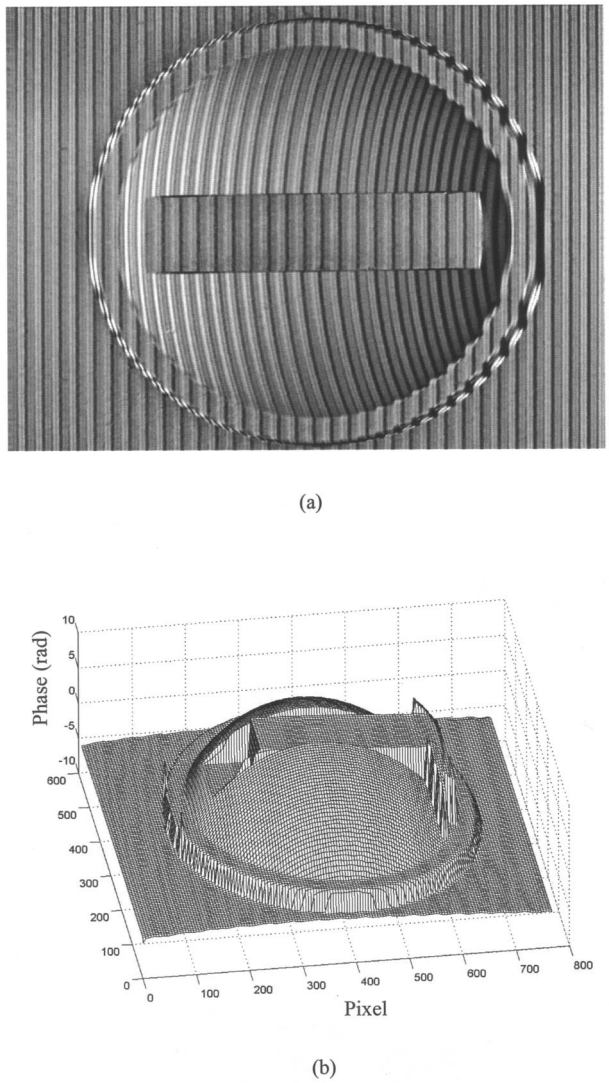

Fig. 8. (a) SFM map (without fitting error modification); (b) 3D plot shape generated by SFM-guided unwrapping (without fitting error modification).

would be able to reflect the deviation of the fringe pattern from the theoretical fringe pattern. In the following subsection, a 9×3 pixel window is used to calculate the SFM and $E(x, y)$.

B. Surface Profile of Test Specimen

The surface profile of a hemisphere specimen recovered by Goldstein, TFM-guided, SFM-guided, and fitting-error modified SFM-guided algorithms is discussed in this section. Four 90° phase-shifted vertical fringe patterns are projected onto the object surface, and Fig. 1 shows an image of the fringe patterns. A wrapped phase map obtained by a four-step phase-shifting algorithm is shown in Fig. 5. There is a groove at the center of the hemisphere, which presents a challenge in the recovery of the actual surface profile. In order to unwrap the phase in the area surrounding the groove, a path would have to go across the groove horizontally. However, a path going across the top or bottom of the groove would produce errors, since there are discontinuous and the phase values are unreliable.

Figure 6(a) shows branch cuts generated by Goldstein's algorithm. Two branch cuts are generated to balance four residues at the top and bottom of the groove. The branch cuts are placed vertically instead of horizontally, since short branch-cuts are generated with priority in Goldstein's algorithm. However, they prevent a horizontal unwrapping path; thus errors occur when the path is forced to go across the top or bottom of the groove. An erroneous 3D plot of the surface profile, as shown in Fig. 6(b), is obtained.

Figure 7(a) is a TFM map derived from four phase-shifted fringe patterns. The TFM accurately reflects the phase quality in most parts of the image. Flat surface areas are of high quality, and areas around the border of the hemisphere are of low quality. However, the TFM values are high at the top of the groove (highlighted by arrows), where the phase data

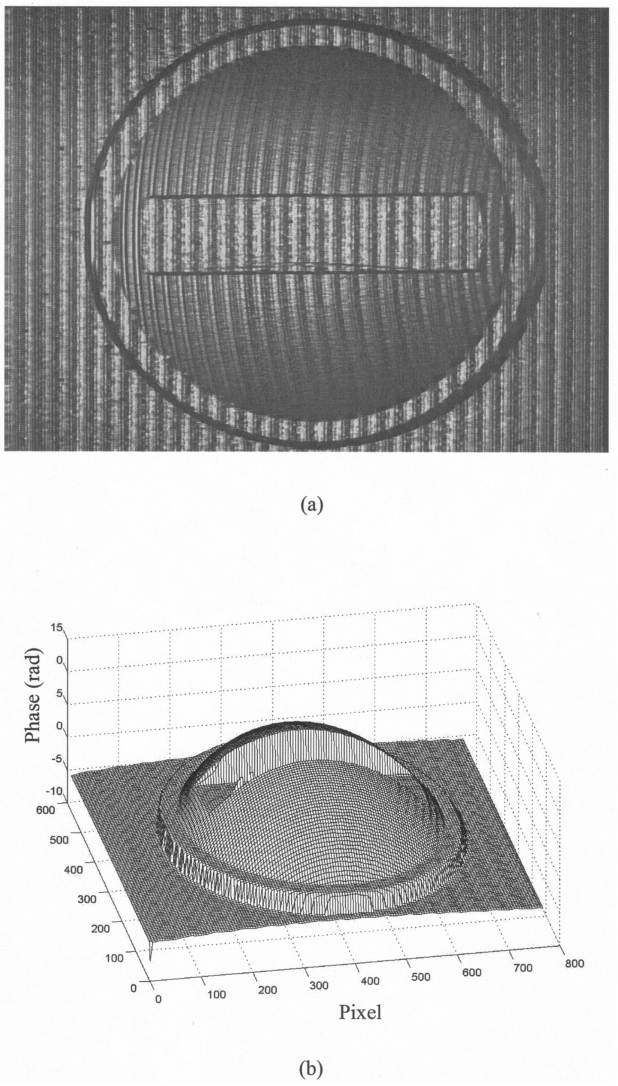

Fig. 9. (a) SFM map (with fitting error modification); (b) 3D plot shape generated by the SFM-guided unwrapping (with fitting error modification).

are unreliable. This result is caused by the illumination setup, which does not produce enough shadow. Consequently, the TFM is not able to identify the change in profile. The 3D plot in Fig. 7(b) shows errors similar to those in Fig. 6(b).

Figure 8(a) is a SFM map derived from a single fringe pattern. The SFM clearly identifies changes in the y-direction profiles at the top and bottom of the groove but encounters problems in identifying changes in the x direction. The SFM values fluctuate widely at the edge of the hemisphere and are unreasonably high at the right end of the groove. The 3D plot in Fig. 8(b) shows the errors at the right end of the groove, where phase qualities are wrongly identified.

Figure 9(a) shows a fitting-error modified SFM map, in which both x- and y-direction changes in profile are detected. Compared with Fig. 8(a), the SFM values at the edge of the hemisphere and at the right end of the groove decrease. Figure 9(b) shows the surface profile obtained. As can be seen, the profiles are correctly generated without the errors introduced by the other methods.

4. Concluding Remarks

It is shown that fitting-error modified spatial fringe modulation (SFM) is a good phase quality indicator. It is capable of identifying both x- and y-direction changes in surface profile. Unlike TFM, SFM is derived from a single fringe pattern; thus, it is a suitable method for fringe analysis in dynamic measurement. Furthermore, the SFM value of a point under consideration is calculated from its $N \times M$ neighboring pixels' grey levels, and the spatial connection among these points is well reflected, which makes the SFM less dependent on illumination than TFM. Owing to the unique shape of the specimen, SFM-guided phase unwrapping shows better result than that obtained by a block path and the TFM-guided unwrapping algorithm.

References

1. C. Quan, X. Y. He, C. F. Wang, C. J. Tay, and H. M. Shang, "Shape measurement of small objects using LCD fringe projection with phase shifting," Opt. Commun. **189,** 21–29 (2001).
2. B. K. A. Ngoi, K. Venkatakrishnan, N. R. Sivakumar, and T. Bo, "Instantaneous phase shifting arrangement for microsurface profiling of flat surface," Opt. Commun. **190,** 109–116 (2001).
3. Y. B. Choi and S. W. Kim, "Phase-shifting grating projection moiré topography," Opt. Eng. **37,** 1005–1010 (1998).
4. J. Strand and T. Taxt, "Performance evaluation of two-dimensional phase unwrapping algorithms," Appl. Opt. **38,** 4333–4344 (1999).
5. D. C. Ghiglia and M. D. Pritt, *Two-Dimensional Phase Unwrapping: Theory, Algorithms, and Software* (Wiley, New York, 1998).
6. R. M. Goldstein, H. A. Zebker, and C. L. Werner, "Satellite radar interferometry: two-dimensional phase unwrapping," Radio Sci. **23,** 713–720 (1988).
7. D. J. Bone, "Fourier fringe analysis: the two-dimensional phase unwrapping problem," Appl. Opt. **30,** 3627–3632 (1991).
8. J. A. Quiroga, A. Gonzalez-Cano, and E. Bernabeu, "Phase-unwrapping algorithm based on an adaptive criterion," Appl. Opt. **34,** 2560–2563 (1995).
9. H. Lim, W. Xu, and X. Huang, "Two new practical methods for phase unwrapping," in *Proceedings of the 1995 International Geoscience and Remote Sensing Symposium* (IEEE, Piscataway, N.J., 1995), pp. 196–198.
10. W. Xu and I. Cumming, "A region growing algorithm for InSAR phase unwrapping," in *Proceedings of the 1996 International Geoscience and Remote Sensing Symposium* (IEEE, Piscataway, N.J., 1996), pp. 2044–2046.
11. M. W. Roth, "Phase unwrapping for interferometric SAR by the least-error path," Johns Hopkins University Applied Physics Lab Technical Report, Laurel, Md., 30 March (1995).
12. M. D. Pritt, "Phase unwrapping by means of multigrid techniques for interferometric SAR," IEEE Trans. Geosci. Remote Sess. **34,** 728–738 (1996).
13. B. Ströbel, "Processing of interferometric phase maps as complex-valued phasor images," Appl. Opt. **35,** 2192–2198 (1996).
14. W. Li and X. Y. Su, "Phase unwrapping algorithm based on phase fitting reliability in structured light projection," Opt. Eng. **41,** 1365–1372 (2002).